



## Influence of the synthesis route on the properties of BNBT ceramics

Elisa Mercadelli, Alessandra Sanson, Claudio Capiani, Anna Luisa Costa, Carmen Galassi\*

CNR-ISTEC, Institute of Science and Technology for Ceramics, National Research Council,  
via Granarolo 64, 48018 Faenza, Italy

Received 1 October 2008; received in revised form 16 March 2009; accepted April 27 2009

### Abstract

BNBT ( $0.94[(\text{Bi}_{0.5}\text{Na}_{0.5})\text{TiO}_3]-0.06\text{BaTiO}_3$ ) nanopowders were prepared starting from an aqueous solution of inorganic salts (barium acetate, bismuth nitrate, sodium nitrate and titanium isopropoxide) either by the citrate-nitrate sol-gel combustion (SGC) or by spray drying (SD). Their chemical and microstructural properties were compared with the ones of the same system obtained by mechanical mixing of oxides (SSCO). The SD and SGC powders require temperatures 150 and 300°C lower than SSCO powder to form the perovskite phase. The chemical and physical properties of the obtained powders strongly depend on the considered chemical route. Therefore the subsequent sintering step and consequently the microstructure of the obtained ceramics differ significantly. The microstructures as well the piezoelectric properties of the sintered SGC, SD, SSCO samples are investigated and a critical comparison is presented.

**Keywords:** sol-gel combustion, spray drying, nanopowders, microstructure, piezoelectric characterization

### 1. Introduction

Among piezoelectric ceramics, materials based on lead zirconate titanate solid solution  $\text{Pb}(\text{Ti},\text{Zr})\text{O}_3$  (PZT) exhibit the best piezoelectric properties and are the most widely used [1–3]. However, the research has been recently focused on lead free compositions [4,5], as a consequence of environmental issues connected with the lead toxicity.

The solid solution between bismuth sodium titanate,  $(\text{Bi}_{0.5}\text{Na}_{0.5})\text{TiO}_3$ , and barium titanate,  $\text{BaTiO}_3$ , is considered as one of the most promising lead-free piezoelectric materials [6]. However, the stoichiometry of this system must be carefully controlled in order to obtain a composition lying in the rhombohedral ( $F_\alpha$ )-tetragonal ( $F_\beta$ ) morphotropic phase boundary (MPB) and consequently to fully exploit its piezoelectrical potentials [7].

Recently, the so called “chemical methods” have attracted considerable attention of many researchers. The use of precursors solution, in fact, leads to very homogeneous nano-structured powders with higher reactivity than those produced by the conventional solid state reaction. This characteristic allows a sensible reduction in the temperature of perovskite phase formation

and milder sintering conditions limiting in this way the loss of volatile  $\text{Bi}_2\text{O}_3$  and  $\text{Na}_2\text{O}$ .

Several chemical methods, like aqueous citrate gel [8–11], conventional sol-gel [12,13], hydrothermal synthesis [14–16], stearic acid gel [17] and mechanochemical synthesis [18] were applied for obtaining NBT and NBT-based ceramic powders.

Among these methods, aqueous-based spray drying [19] and sol-gel combustion [20] are relatively simple and low-cost techniques to produce very fine powders with a close control of the stoichiometry and well determined physical and morphological properties.

The spray-drying process is divided in four principal phases: i) atomization of the solution and mixing with the air flowing in a hot chamber, ii) evaporation of a liquid phase from the obtained droplets iii) drying of the formed particles and iv) separation of the dried particles from the air flow. All these steps contribute to the final morphology of the particles and must be controlled.

The citrate sol-gel combustion combines the advantages of the sol-gel chemistry with the combustion process, and leads to produce homogeneous and highly reactive crystalline powders without the intermediate decomposition and/or calcining steps required by other chemical synthesis routes.

\* Corresponding author: tel: +39 05 46 699750  
fax: +39 05 46 46381, e-mail: carmen.galassi@istec.cnr.it

In this study  $0.94[(\text{Bi}_{0.5}\text{Na}_{0.5})\text{TiO}_3]-0.06\text{BaTiO}_3$  powders were synthesized by the citrate-nitrate sol-gel combustion (SGC), spray drying (SD) and solid state synthesis from carbonate and oxides (SSCO). The microstructure as well as the piezoelectric properties of the sintered SGC, SD, SSCO samples were investigated and a critical comparison is presented.

## II. Experimental

In Fig. 1 the flow charts relative to the different experimental procedures used are presented.  $\text{Ti}[\text{OCH}(\text{CH}_3)_2]_4$  (97%, Aldrich),  $\text{Ba}(\text{CH}_3\text{COO})_2$  (99%, Merck),  $\text{Bi}(\text{NO}_3)_3 \cdot 5\text{H}_2\text{O}$  (98%, Aldrich) and  $\text{NaNO}_3$  (99.5%, Carlo Erba) were used as raw materials in SD and SGC precursor solution.

In SD route, the metal salts were dissolved under stirring in nitric acid (Carlo Erba reagents, 65 wt.%) in presence of hydrogen peroxide (Riedel de Haen, 30%). The as-prepared solution was sprayed and dried in a Labplant SD-05 spray drier at  $220^\circ\text{C}$ . The powder was then calcined at  $650^\circ\text{C}$ , grounded and sieved.

In SGC, citric acid monohydrate (>99%, Merck) was used as both chelating agent and fuel for the combustion process. Nitric acid solution was used to dissolve all the starting metal salts, with molar ratios of citrate/nitrate (C/N) equal to 1. Citric acid monohydrate was then dissolved into the acid solutions to obtain a molar ratio of citric acid to metal cations equal 2.5 : 1. The resulting solution was heated under stirring at  $80^\circ\text{C}$  to evaporate the exceeding solvent and to form a transparent orange-yellow gel. The addition of urea (a molar ratio of urea to metal cations was 1.4 : 1) prevents the precipitation of metal-citrate compounds as a consequence of pH variations induced by the evaporation of  $\text{NH}_3$ . The prepared gel was heated at  $500^\circ\text{C}$  to obtain the perovskite phase.

For SSCO route the stoichiometric amount of  $\text{BaCO}_3$  (99.4%, Merck), and  $\text{TiO}_2$  (99.4%, Degussa),  $\text{Na}_2\text{CO}_3$  (99.5%, Merck),  $\text{Bi}_2\text{O}_3$  (99.9%, Aldrich) were ball milled in water for 48 h. Water was removed by freeze-drying and the powder sieved at  $400\ \mu\text{m}$ . The SSCO powder was then calcined at  $800^\circ\text{C}$ , grounded and sieved.

The SD, SGC and SSCO BNBT powders were uniaxially ( $650\ \text{Kg}/\text{cm}^2$ ) and isostatically ( $3000\ \text{Kg}/\text{cm}^2$ ) pressed in thin disks (30 mm diameter and 1 mm thickness) and sintered at  $1100\text{--}1150^\circ\text{C}$  for 2 h.

The chemical composition of the precursor solutions and combusted powders was determined by inductively coupled plasma-atomic emission spectrometry (ICP-AES) (Liberty 200, Varian, Clayton South, Australia). The thermogravimetry (TGA) and differential thermal analyses (DTA) were carried out at a heating rate of  $10^\circ\text{C}/\text{min}$  using a simultaneous thermal analyser (STA 409, Netzsch, Selb/Bavaria, Germany). Phase purity was tested by X-ray diffractometer (XRD) with a Miniflex Rigaku (Japan) system operating with Ni filtered  $\text{CuK}\alpha$  radiation. The powder morphology was investigated by scanning electron microscopy (SEM) (Leica Cambridge Stereoscan 360) coupled with an energy-dispersive X-ray spectrometer (EDS). Infrared spectra of the precursor powders and of heated powders at different temperatures were recorded in the range  $400$  to  $4000\ \text{cm}^{-1}$ , using a Fourier transform infrared spectrometer (FTIR) (Perkin-Elmer 1700). Electrical measurements were carried out on the sintered samples electroded with silver paste and poled at  $3\ \text{kV}/\text{mm}$  and  $120^\circ\text{C}$  for 40 min. An HP4194 impedance analyser was used to determine the piezoelectric constants. The electrical characterization at low field (0.5 V) was performed on the disk shaped samples (electroded perpendicularly to the direction of the applied pressure) following the standard IEEE 176-1987 and CENELEC 50324. The elasto-

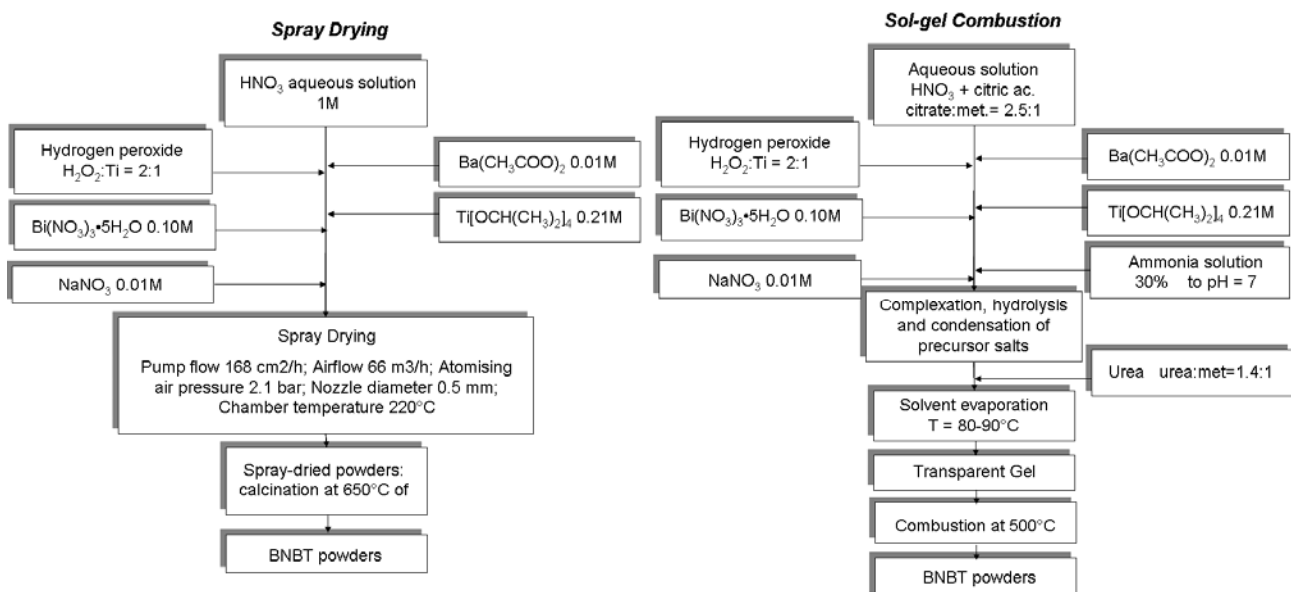


Figure 1. Scheme of the synthesis of the BNBT powders: SD and SGC routes

piezo-dielectric constants were calculated from the values of resonance and antiresonance frequencies of the planar mode (maximum conductance -  $f_s$  and maximum resistance -  $f_p$ ), minimum impedance and capacitance. The  $d_{33}$  constant was directly measured by a  $d_{33}$ -meter S5865, Sinocera on the same samples.

### III. Results and discussion

The composition of the SGC and SD powders was controlled after every critical step of the process and resulted constant throughout the synthesis path keeping the expected stoichiometric ratios.

The DTA and TGA curves of the SD precursor powder and SGC precursor gel are compared in Fig. 2. The SD mixture of nitrates evolves with endothermic reactions that under 200°C are attributed to water and titanium isopropoxides decomposition, whilst at higher temperatures (420–500°C) they are attributed to nitrates decomposition [19]. The endothermic peak at 650°C is related to the formation of the solid solution of interest. On the other hand, the SGC precursor gel is subjected only to exothermic reactions (except for small endothermic peaks related to the evaporation of the adsorbed water). The exothermic peak centred at the lowest temperature (250°C) is attributed to the auto-ignition redox reaction between fuel and oxidizer responsible for the greater part of the weight loss, while the peaks at 440 and 500°C can be related to the decomposition of residual organics and to the perovskite phase formation. The total weight loss was then 30% for the SD powder and 70% for the SGC precursor gel.

The FT-IR spectra of SGC and SD powders treated at different temperatures are shown in Fig. 3. Before calcination/combustion, both samples present the typical vibrations of  $\text{NO}_3^-$  ions at  $825\text{ cm}^{-1}$  and at  $1384\text{ cm}^{-1}$  and  $\text{NO}_2$  asymmetric and symmetric stretching (around  $1600$  and  $1380\text{ cm}^{-1}$ ). In addition, the SGC sample shows, the bands at  $\sim 1400\text{ cm}^{-1}$  (hidden by an intense band of nitrate ions centred at  $1384\text{ cm}^{-1}$ ) and at  $1635\text{ cm}^{-1}$ , that can be assigned to symmetric and asymmetric stretching vibration of  $[\text{COO}]^-$  and the very small band at  $1717\text{ cm}^{-1}$  assigned to the C=O stretching mode of an ester bond. These two bands can be related to the formation of the metal citrate complex during synthesis. Moreover the band at  $3144\text{ cm}^{-1}$ , related to the OH stretching vibration, is due to the unreacted citric acid.

The intensity of these bands decreases progressively with temperature: the ones related to the residual carbo-nitro compounds disappear in the SD sample calcined at  $650^\circ\text{C}$  and in the SG sample combusted at  $500^\circ\text{C}$ , while the bands related to the adsorbed water molecules ( $3440$  and  $1630\text{ cm}^{-1}$ ) and Ti-O bond ( $640\text{ cm}^{-1}$  [21]) are present in the spectrum of both SG and SD calcined powders.

The XRD patterns of the powders treated at different temperatures are shown in Fig. 4. The powder processed via spray-drying shows the formation of pure perovskite phase at  $650^\circ\text{C}$ . The system passes through the

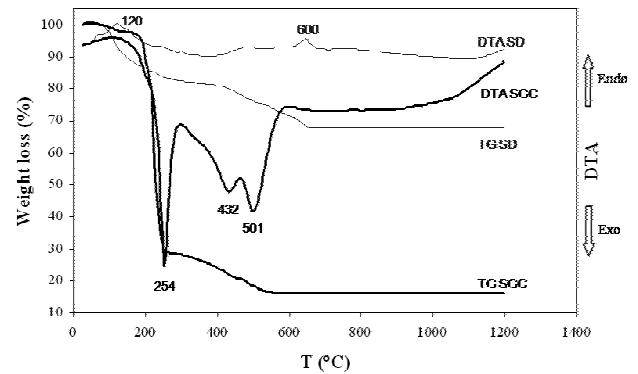


Figure 2. Thermal analysis TG-DTA of the SD precursor powder and SGC precursor gel dried at  $220$  and  $100^\circ\text{C}$  respectively

formation of the more stable pyrochlore phase: in fact the most intense peak ( $2\theta = 30$ ) that is observed at  $350^\circ\text{C}$ , in addition to the amorphous phase, converts to perovskite phase between  $550$  and  $600^\circ\text{C}$ . The XRD diffractograms of the SGC powder show that combustion at  $300$  and  $400^\circ\text{C}$  leads to amorphous powders. An initiation temperature higher than  $400^\circ\text{C}$  is needed to directly induce the crystallization of the pure perovskite phase (except for a very small amount of metastable pyrochlore phase). On the other side, the SSCO powder is fully reacted only after calcination at  $800^\circ\text{C}$ .

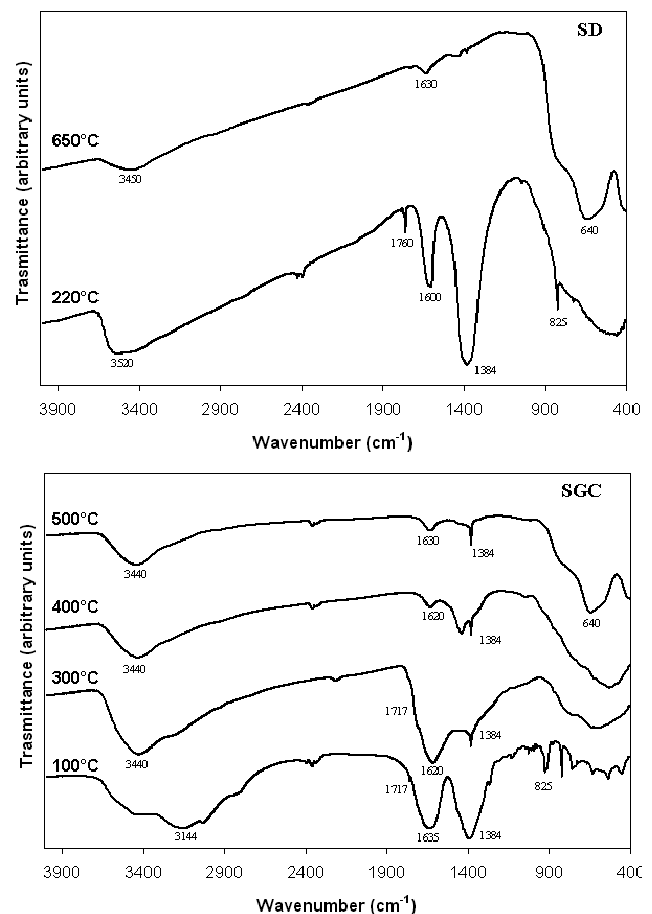


Figure 3. FT-IR spectra of SGC and SD powders treated at different temperatures

The morphologies of the as-sprayed and as-combusted powders are shown in Fig. 5. The as-combusted powders are nanostructured, but show high aggregates that preserve the lamellar structure deriving from the gel polymeric network. On the other hand, spherical and hollow aggregates of highly reactive nanometric particles are produced by SD method. The Table 1 summarizes the values of specific surface area and mean particle size of the BNBT powders obtained from three techniques. The values of specific surface area correspond to nominal primary particle size of around 200 nm for the SD and SSCO powders and 70 nm for the SGC powders [22]. The aggregation degree of primary particles is particularly evident for the SD particles as mean diameter size reveals (6.6  $\mu\text{m}$ ). The unavoidable aggregation of primary particles occurs during the thermal treatment of precursor powders necessary to produce a pure perovskite phase. The high specific surface area obtained from SGC is a consequence of the big amount of gas ( $\text{CO}_2$ ,  $\text{NO}_x$ ) developed during the combustion process.

The microstructures of the sintered SGC, SD and SSCO samples are shown in Fig. 6. The SD sample presents two areas named A and B that differ from the matrix characterized, respectively, by elongated grains (A) and smaller grain size (B). The EDS analysis reveals that, in comparison to the matrix phase, the composition of A zone is Ba rich, whilst the composition of B zone is Bi rich. The SGC sample shows a homogeneous microstructure without inclusion and with mean grain size comparable to that of the starting powder. Fully dense areas change to large pores as a consequence of presintered zone present in the as-combusted powder. The SSCO sample shows a bimodal microstructure with a fraction of large grains of about 20  $\mu\text{m}$  within a fine sized grain matrix (of about 2  $\mu\text{m}$ ), most probably due to non homogeneous size distribution in the starting powder.

The large differences between microstructures obtained through different processes could be explained on the basis of chemical and physical properties of the starting BNBT powder. The evolution of nanostructures

**Table 1.** Values of specific surface area and  $D_{50}$  of SD, SGC and SSCO powders

Powders	Specific surface area [ $\text{m}^2/\text{g}$ ]	$D_{50}$ [ $\mu\text{m}$ ]
SD	4.8	6.6
SGC	15.0	1.0
SSCO	4.8	0.9

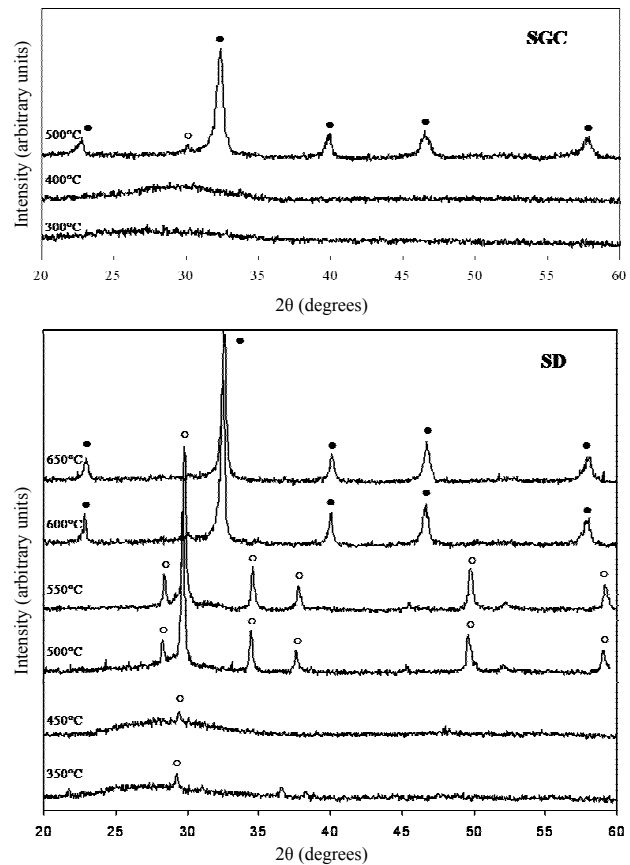


**Figure 4.** XRD patterns of the powders treated at different temperatures [(●) perovskite phase, (○) pyrochlore]

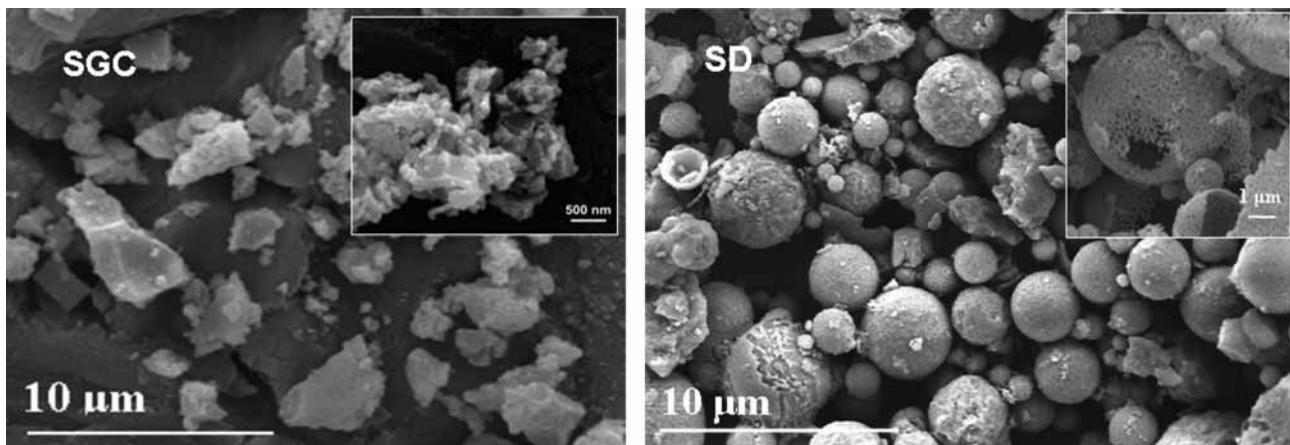


**Figure 5.** SEM micrographs of the as-spray dried powder (SD) at 220°C and of the as-combusted powder (SGC) at 500°C

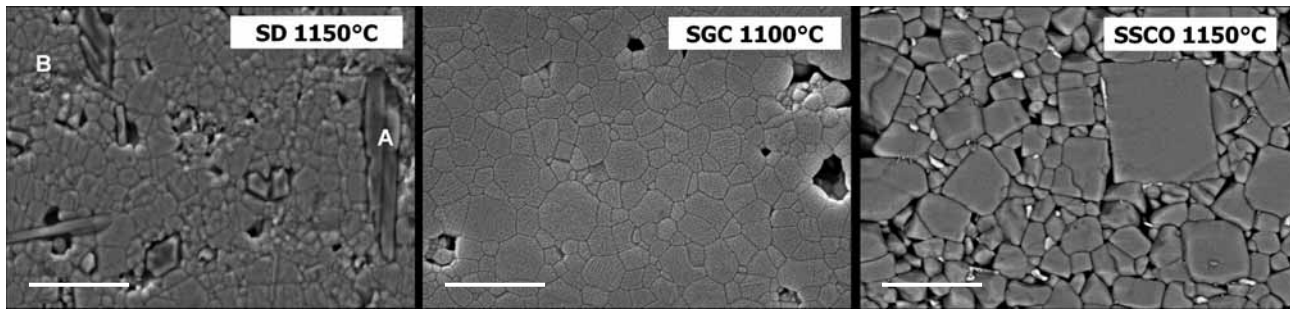


Figure 6. SEM micrographs of polished and etched surfaces of the sintered SD, SGC and SSCO samples (bar = 10 µm)

during the process is strictly connected to the reduction of the high surface energy. Several processes are involved in this reduction: at atomic level (composition segregation or enrichment of impurities on the surface), at level of individual structures (shaping of nanoparticles structures) and at overall system level (sintering, Ostwald ripening) [23]. All these processes are especially active in nanoparticle systems because solid state diffusion mechanisms involved are promoted by high surface energy and short diffusion distance. In particular, phenomena of phase segregation at surface level together with partial sintering can occur also at low temperature heavily influencing the nanostructures during the calcination or combustion steps. The partial sintering can be explained by the low surface area of the SD powder after calcination whilst the segregation of BaO at surface level could explain the formation of Ba rich phase (zone A, Fig. 6) during sintering. Furthermore, evaporation and condensation of high volatile  $\text{Na}_2\text{O}$  could leave Bi rich phase (zone B, Fig. 6) inside matrix. The SGC combusted powder seems to be less influenced by these mechanisms, most probably because the temperature reached in the fast combustion step (higher than that set in the oven) is high enough to promote the direct formation of perovskite phase without involving the phase evolution steps that occur during the calcination of the as-sprayed powder (Fig. 4).

The piezoelectric properties are summarized in Table 2. The segregation of Ba and Bi rich zones in the SD sintered sample causes a decrease of its piezoelectric performances. The stoichiometry of the system, in fact is crucial to obtain suitable piezoelectrical properties. Nevertheless, despite a very different microstructure, the materials show comparable piezoelectric properties: further investigations will be carried out to better understand the correlation between piezoelectric properties and BNBT microstructures.

Table 2. Piezoelectric properties of SD, SGC and SSCO samples

Sample	Density, $\rho$ [%]	$\epsilon_{33}^T$	$k_p$	$d_{31}$ [ $10^{-12}$ m/V]	$d_{33}$ [ $10^{-12}$ m/V]
SD	96.6	610	0.267	-34.8	118
SGC	97.1	698	0.272	-38.6	125
SSCO	96.1	648	0.265	-36.8	131

#### IV. Conclusions

BNBT sintered samples were prepared following two chemical routes and comparing the results with samples obtained by solid state synthesis.

The spray drying from salts solution (SD) and sol gel combustion synthesis (SGC) were considered. The nanostructures of the powders are strongly dependent on the considered chemical route. The as-combusted powders are nanostructured, but show high degree of agglomeration with a lamellar structure deriving from the gel polymeric network. On the other hand, spherical and hollow aggregates of highly reactive nanometric particles are produced by SD. The nanostructured powders obtained by chemical routes require 150 and 300°C lower temperature than the SSCO powder to form the perovskite phase. Nevertheless, the high reactivity of the as-sprayed powder generates phenomena of pre-sintering and phase segregation at surface level during calcination that influences negatively the final microstructure of sintered samples. The SGC samples show an uniform microstructure as a consequence of higher stability of starting powder produced by a rapid heating at high temperature. The materials show comparable piezoelectric properties, but the SGC sample densifies at lower temperature.

**Acknowledgements:** This research work was presented at the 4th workshop of COST 539 Action – ELENA “Fabrication, Properties & Applications of Electroceramic Nanostructures” held in Genoa, June 26–28, 2008. Therefore the COST 539-Action is gratefully acknowledged.

#### References

1. A. Ballato, “Piezoelectricity: History and new thrusts”, *IEEE Ultrasonics Symposium*, (1996) 575–583.
2. N. Setter, *Piezoelectric Materials in devices*, Ceramics Laboratory, EPFL, 2002.

3. B. Jaffe, W.R. Cook, H. Jaffe *Piezoelectric Ceramics*, Academic Press, London 1971.
4. M.D. Maeder, D. Damjanovic, N. Setter, “Lead free piezoelectric materials”, *J. Electroceram.*, **13** (2004) 385–392.
5. T. Takenaka, H. Nagata, “Current status and prospects of lead-free piezoelectric ceramics”, *J. Eur. Ceram. Soc.*, **25** (2005) 2693–2700.
6. T. Takenaka, K. Maruyama, K. Sakata, “ $(\text{Bi}_{1/2}\text{Na}_{1/2})\text{TiO}_3$ - $\text{BaTiO}_3$  system for lead-free piezoelectric ceramics”, *Jpn. J. Appl. Phys., Part 1*, **30** (1991) 2236–2239.
7. H. Yan, D. Xiao, P. Yu, J. Zhu, D. Lin, G. Li, “The dependence of the piezoelectric properties on the differences of the A-site and B-site ions for  $(\text{Bi}_{1-x}\text{Na}_x)\text{TiO}_3$ -based ceramics”, *Mater. Design*, **26** (2005) 474–478.
8. D.L. West, D.A. Payne, “Preparation of  $0.95(\text{Bi}_{1/2}\text{Na}_{1/2})\text{TiO}_3 \cdot 0.05\text{BaTiO}_3$ ”, *J. Am. Ceram. Soc.*, **86** (2003) 192–194.
9. Q. Xu, S. Chen, W. Chen, D. Huang, J. Zhou, H. Sun, Y. Li, “Synthesis of  $(\text{Na}_{0.5}\text{Bi}_{0.5})\text{TiO}_3$  and  $(\text{Na}_{0.5}\text{Bi}_{0.5})_{0.92}\text{Ba}_{0.08}\text{TiO}_3$  powders by a citrate method”, *J. Mater. Sci.*, **41** (2006) 6146–6149.
10. C. Y. Kim, T. Sekino, K. Niihara, “Synthesis of bismuth sodium titanate nanosized powders by solution/sol-gel process”, *J. Am. Ceram. Soc.*, **86** (2003) 1464–1467.
11. A. Kundu, A.N. Soukhovjak, “Ba-Zr codoped sodium bismuth titanate by novel alkoxyless wet chemical route: processing and electromechanical behavior”, *Appl. Phys. A: Mater. Sci. Process*, **82** (2006) 309–315.
12. S. Saïd, J.P. Mercurio, “Relaxor behaviour of low lead and lead free ferroelectric ceramics of the  $\text{Na}_{0.5}\text{Bi}_{0.5}\text{TiO}_3$ - $\text{PbTiO}_3$  and  $\text{Na}_{0.5}\text{Bi}_{0.5}\text{TiO}_3$ - $\text{K}_{0.5}\text{Bi}_{0.5}\text{TiO}_3$  systems”, *J. Eur. Ceram. Soc.*, **21** (2001) 1333–1336.
13. M.-L. Zhao, C.-L. Wang, J.-F. Wang, H.-C. Chen, W.-L. Zhong, “Enhanced piezoelectric properties of  $(\text{Bi}_{0.5}\text{Na}_{0.5})_{(1-x)}\text{Ba}_x\text{TiO}_3$  lead-free ceramics by sol-gel method”, *Acta Physica Sinica*, **53** (2004) 2357–2362.
14. Y.J. Ma, J.H. Cho, Y.H. Lee, B.I. Kim, “Hydrothermal synthesis of  $(\text{Bi}_{1/2}\text{Na}_{1/2})\text{TiO}_3$  piezoelectric ceramics”, *Mater. Chem. Phys.*, **98** (2006) 5–8.
15. J.-H. Cho, Y.-J. Ma, Y.-H. Lee, M.-P. Chun, B.-I. Kim, “Piezoelectric ceramic powder synthesis of bismuth-sodium titanate by a hydrothermal process”, *J. Ceram. Process. Res.*, **7** (2006) 91–94.
16. X. Jing, Y. Li, Q. Yin, “Hydrothermal synthesis of  $\text{Na}_{0.5}\text{Bi}_{0.5}\text{TiO}_3$  fine powders”, *Mater. Sci. Eng. B: Solid State Mater. Adv. Technol.*, **99** (2003) 506–510.
17. J. Hao, X. Wang, R. Chen, L. Li, “Synthesis of  $(\text{Bi}_{0.5}\text{Na}_{0.5})\text{TiO}_3$  nanocrystalline powders by stearic acid gel method”, *Mater. Chem. Phys.*, **90** (2005) 282–285.
18. H.A.M. van Hal, W.A. Groen, S. Maassen, W.C. Keur, “Mechanochemical synthesis of  $\text{BaTiO}_3$ ,  $\text{Bi}_{0.5}\text{Na}_{0.5}\text{TiO}_3$  and  $\text{Ba}_2\text{NaNb}_5\text{O}_{15}$  dielectric ceramics”, *J. Eur. Ceram. Soc.*, **21** (2001) 1689–1692.
19. A. Sanson, C. Galassi, A.L. Costa, U. Russo, “Synthesis of  $0.94(\text{Bi}_{1/2}\text{Na}_{1/2})\text{TiO}_3$ - $0.06\text{BaTiO}_3$  by spray-drying”, *Proc. Ferroelectrics UK Sheffield*, UK (2001) 119–126.
20. E. Mercadelli, C. Galassi, A.L. Costa, S. Albonetti, A. Sanson “Sol-gel combustion synthesis of BNBT powders”, *J. Sol-Gel Sci. Technol.*, **46** (2008) 39–45.
21. S. Music, M. Gotic, M. Ivanda, S. Popovic, A. Turkovic, R. Trojko, A. Sekulic, K. Furic, “Chemical and microstructural properties of  $\text{TiO}_2$  synthesized by sol-gel procedure”, *Mater. Sci. Eng. B: Solid State Mater. Adv. Technol.*, **47** (1997) 33–40.
22. E. Jud, L.J. Gauckler, “Sintering behavior of cobalt oxide doped ceria powders of different particle sizes”, *J. Electroceram.*, **14** (2005) 247–253.
23. G. Cao, *Nanostructures and nanomaterials - Synthesis, properties, and applications*, Imperial College Press, 2004.